Revealing Topological Structure in the $SU(2)$ Vacuum

Thomas DeGrand, Anna Hasenfratz, and Tamás G. Kovács
Department of Physics
University of Colorado, Boulder CO 80309-390

February 2008

Abstract

In this paper we derive a simple parametrization of the cycling method developed by us in our earlier work. The new method, called renormalization group (RG) mapping, consists of a series of carefully tuned APE-smearing steps. We study the relation between cycling and RG mapping. We also investigate in detail how smooth instantons and instanton-anti-instanton pairs behave under the RG mapping transformation. We use the RG mapping technique to study the topological susceptibility and instanton size distribution of SU(2) gauge theory. We find scaling in both quantities in a wide range of coupling values. Our result for the topological susceptibility, $\chi^{1/4} = 220(6)$ MeV, agrees with our earlier results.

arXiv:hep-lat/9711032v1 17 Nov 1997

1 Introduction

Instantons are an important part of the QCD vacuum. They are expected to play a major role in chiral symmetry breaking and the low energy hadron spectrum [1, 2], in addition to explaining the U(1) problem [3, 4]. For the latter the value and scaling properties of a global observable, the topological susceptibility

$$\chi_{top} = \frac{\langle Q^2 \rangle}{V}$$

is needed, while for describing chiral symmetry breaking the size and spatial distribution of the instantons are also important.

Lattice Monte Carlo simulation is the only available non-perturbative method to study the topology of the QCD vacuum from first principles. Since the instantons carry a very small portion of the vacuum energy, on typical lattice configurations they are hidden by the vacuum fluctuations. This makes their study using lattice methods quite difficult. To overcome this problem, lattice studies either smooth the configurations by some direct method while trying to preserve the underlying topological structure, use non-local observables that effectively and intelligently do the smoothing, or combine the two. Examples for non-local observables are the the renormalization group inspired minimization method [5, 6] and the methods that use fermionic observables and relate the topological charge of a configuration to the index of the Dirac operator through the Atiyah-Singer index theorem [7, 8]. Examples for direct smoothing are our cycling [9] procedure or the different cooling techniques used by many different groups [10, 11, 12]. All of these methods have an intrinsic cutoff in the minimum instanton size they can identify before it falls through the lattice. In addition, nearby instanton-anti-instanton pairs might disappear from the lattice during smoothing or become otherwise invisible to the measuring algorithm. Nevertheless one expects that as the continuum limit is approached and typical instanton sizes grow in lattice units, all these methods will give the same result.

In several recent papers [6, 9] we studied lattice topology using a method based on the renormalization group equation. This method has the advantage of keeping instantons above a certain size of approximately one lattice spacing intact both in location and size, and preserving nearby pairs as well. However the method involves an "inverse blocking" step where the original lattice is mapped through a minimization step into a fine lattice with half the lattice spacing and twice the lattice size. This makes the method very slow and memory intensive. Using the RG method at fairly coarse lattice spacing, combined with a scale invariant SU(2) fixed point (FP) action, we measured the topological susceptibility and the instanton size distribution.

We found $\chi^{1/4} = 230(10)$ MeV and from the size distribution we concluded that the average instanton in SU(2) has a radius of about 0.2 fm. These values differ from the results obtained by other groups. Both the improved cooling method [12] and the "heating method" of the Pisa group [13] find a consistently smaller susceptibility, $\chi^{1/4} = 198(8)$ MeV, which translates into about a factor of 2 difference in the expectation value of Q^2. In addition, the size distribution of Ref. [12] peaks at about $\bar{\rho} = 0.43$ fm, more than twice our value.

It is essential to resolve the differences between the different methods. In this paper we develop a procedure called renormalization group mapping (or RG mapping) to approximate the cycling process of Ref. [9] without actually constructing the fine lattice. This way we can study larger lattices and perform more reliable scaling tests. We have performed several tests, both on smooth instantons and Monte Carlo configurations, to understand and control the properties of the RG mapping method. In order to compare our results directly with those of Refs. [12, 14], we have also decided to use the Wilson action instead of our FP gauge action in this study.

All direct smoothing transformations distort the original lattice configuration. This makes the extraction of (continuum) short to medium distance physics, like observations of topological objects, very delicate. If any space-time symmetric smoothing transformation iis repeated enough times, all the vacuum structure in any finite volume, including the simulation volume, will be washed away. Thus, it does not make sense to extrapolate one's results to the limit of a very large number of smoothing steps. The only measurements which are physically meaningful are measurements which are extrapolated back to the original lattice, that is, back to zero smoothing steps. This requires careful monitoring of observables over the whole history of smoothing transformations.

(The measurement of a long-distance observable, like a mass, is more robust because one can design a smoothing algorithm which preserves the spectrum of the transfer matrix.)

At the end the RG-mapping is a very simple and fast procedure for extracting the topological properties of a lattice configuration, but the price is that all observables must be monitored during the processing and extrapolated back to their values at zero mapping steps.

The rest of the paper is organized as follows. Section 2 describes the RG-mapping procedure and the method by which its parameters are determined. Section 3 shows tests of the RG-mapping method on lattice configurations. Section 4 applies the RG-mapping method to measurements of the topological susceptibility and the properties of instantons. It also includes comparisons with previously published results by us and others. Finally, Section 5 is a summary.

2 Cycling versus RG mapping

The cycling process was discussed in Ref. [9] in detail. It consists of an inverse blocking transformation followed by a blocking step mapping the original lattice to a lattice of the same size and lattice spacing but greatly reduced vacuum fluctuations. Our goal in this section is to develop an approximate mapping from the original configuration to the cycled one without constructing the inverse blocked fine lattice.

2.1 Cycling

The first step of a cycling transformation is an inverse blocking. Inverse blocking identifies the smoothest among the configurations that block back to the original configuration. Technically, one has to solve the steepest descent RG fixed point equation

$$S^{FP}(V) = \min_{\{U\}} \left(S^{FP}(U) + \kappa T(U, V) \right), \tag{1}$$

where $\{U\}$ is the fine configuration with twice the size and half the lattice spacing of the original $\{V\}$ configuration, and $\kappa T(U, V)$ is the blocking kernel [15, 16, 17].

While formally the inverse blocking is non-local, for local FP actions the dependence of the fine links on the original coarse links dies away exponentially with their separation [16] and the mapping $\{V\} \rightarrow \{U(V)\}$ can be considered local. As a consequence, all long distance properties of the coarse and fine configurations are identical, but the fine configuration is locally much smoother than the original one.

Ideally one would like to repeat the inverse blocking step many times until one arrives to a configuration that still has all the long distance properties of the original lattice but the vacuum fluctuations are reduced to a level that the vacuum structure is clearly observable.

Unfortunately this is not practical. The only way to do repeated inverse blocking steps is to map the fine lattice at each step to a smaller lattice without changing the long distance properties or introducing vacuum fluctuations. Since the fine $\{U\}$ configuration has a very subtle coherent structure, a block transformation defined by the original blocking kernel T of Eqn. (1) would bring back most of the vacuum fluctuations. However any other blocking will destroy the coherence and result in a smooth blocked configuration. In Ref. [9] we used a shifted blocking. We did not change the blocking kernel but shifted its origin

to a different sublattice. The shifted transformation has the unpleasant feature (for the present study) that a gauge transformation of the original lattice does not correspond to a gauge transformation on the cycled lattice. In other words, a gauge fixing on the original lattice does not fix the gauge of the cycled lattice. This is not a problem if we work with gauge invariant quantities like closed loops, but in the RG mapping we present here, we are going to map the links of the original lattice to the links of the cycled lattice, and therefore it is important that both lattices be in the same gauge.

It is easy to find a block transformation that preserves the gauge choice, but destroys the coherence of the fine lattice and gives a smooth cycled configuration. In fact any block transformation that is based on the same sublattice as the inverse blocking but has a different kernel than the inverse blocking will do the job. For simplicity we chose a transformation where we first replaced each link by an APE smeared link [18]

$$X_\mu(x) = (1-c)U_\mu(x) \quad + \quad c/6 \sum_{\nu \neq \mu} (U_\nu(x)U_\mu(x+\hat{\nu})U_\mu(x+\hat{\nu})^\dagger$$
$$+ \quad U_\nu(x-\hat{\nu})^\dagger U_\mu(x-\hat{\nu})U_\mu(x-\hat{\nu}+\hat{\mu})), \qquad (2)$$

with $X_\mu(x)$ projected back onto $SU(2)$. Next on the APE transformed lattice we performed a blocking transformation using the same kernel T but with κ equal to infinity, as for the inverse blocking. The parameter c is chosen to mimic the shifted blocking of Ref. [9]. We found that this modified block transformation reduced vacuum fluctuations at the same rate as the shifted blocking when we chose the parameter c=0.75. It also gave the same topological structure as the shifted blocking on several configurations where we performed both procedures.

A cycling step now consists of the following:

$$\{V\}- \text{ inverse blocking } \rightarrow \{U\}- \text{ APE smearing } \rightarrow \{X\}- \text{ blocking } \rightarrow \{W\} \ ,$$

and repeated cycling gives the series

$$\{V\} \rightarrow \{W_1\} \rightarrow \{W_2\} \rightarrow ... \rightarrow \{W_n\}.$$

The lattices $\{V\}$ and $\{W_n\}$ have the same size and lattice spacing but the the vacuum fluctuations are greatly reduced.

2.2 RG mapping

Our goal is to find a mapping from $\{V\}$ to $\{W_n\}$ without doing the minimization of Eqn. (1).

Our new block transformation preserves the gauge. Therefore we require the mapping to do the same. A gauge covariant way to construct the link variables $W_\mu(n)$ of the cycled lattice is to fit them to a linear combination of different paths of the $\{V\}$ links connecting the points n and $n + \mu$. We used 14 different paths with length up to nine links, including the straight connection $V_\mu(n)$ and the length-three staples. From the 14 paths we formed up to 56 combinations and attempted to fit the links of the $\{W\}$ lattice. For each link we fitted the 4 real numbers characterizing each SU(2) matrix in the lattice independently, i.e. we did not constrain them to be an SU(2) element. We created about 20 8^4 lattices generated at lattice spacings $a \approx 0.11$ fm and $a \approx 0.09$ fm for the fit. (We used the FP action of Ref. [9] at $\beta = 1.6$ and $\beta = 1.7$.) It turned out, however, that fits on the independent lattices were consistent and the following fits have been obtained using one $a \approx 0.11$ fm and one $a \approx 0.09$ fm lattices only.

First we start with the mapping $\{V\} \rightarrow \{W_1\}$. The best fit, using 56 operators, had a standard deviation $\sigma^2 \approx 0.014$ per independent variable. If we first performed an APE-smearing $V \rightarrow X$ like Eqn. 2 (of course U is replaced by V), followed by a 56 parameter fit using the smeared X variables as links, the σ^2 was reduced to 0.008. The latter fit reproduced the value of the plaquette on the $\{W\}$ lattice better than 0.5% with a standard deviation per plaquette of about 0.02. (The plaquette expectation value on the $\{W\}$ lattice is between 1.85-1.88.) The topological charge (measured by the FP algebraic operator [9]) was found to be 6×10^{-5} on a charge-0 configuration with standard deviation per site 1.4×10^{-3}.

Is such a complicated mapping really necessary? We tried the mapping $\{V\} \rightarrow \{W_1\}$ using several consecutive APE-smearing steps like Eqn. 2 (again, substitute W for X and V for U). The best fit had $\sigma^2 \approx 0.01$. The details of the APE steps were not very important, as long as each step had $c < 0.5$ and the sum of the c parameters added up to $\sum_i c_i \simeq 1.1$. This simple fit reproduced the plaquette on the $\{W\}$ lattice up to 0.7% and gave the topological charge as 1.2×10^{-4} for a zero charge configuration. The corresponding standard deviations were 0.04 for the plaquette and 1.8×10^{-3} for the topological charge. Since a sequence of simple APE transformations seems to work almost as well as a complicated mapping, in the following we will concentrate on fits using a sequence of APE-smearing transformations.

Next we map $\{V\} \rightarrow \{W_2\}$. The procedure is similar as above. The σ^2 of

this fit is around 0.01 using APE-smearing steps only. Again, the goodness of the APE-smearing fit depended only on the sum of the individual APE steps, $\sum_i c_i = 2.2$ giving the best σ^2. For example, if we do 4 APE smearing steps with $c = 0.45$ followed by a fifth step, the best fit gives $c_5 = 0.4$ with $\sigma^2 = 0.01$. If we do 5 APE steps with $c = 0.4$ first, followed by a fitted sixth step, we get $c_6 = 0.2$ with the same average deviation as before.

We constructed the mappings $\{V\} \rightarrow \{W_n\}$ in a similar way. In Table 1 we list the best parameters together with the appropriate σ^2 values. The parameter values at any given step give the sum of the required APE-smearing steps $\sum_i c_i$. The exact distribution of the c_i parameters have very little effect on the fit quality if each parameter $c_i \leq 0.5$. We found that a series of steps with $c = 0.45$ followed by a last step with $c < 0.45$ to complete the sum $\sum_i c_i$ is a good choice.

It might seem surprising that the quality of the fit actually improves as we fit more times cycled configurations. All that means is that the many times cycled configurations are very smooth, and it is easier to fit a smooth configuration than the rough quantum fluctuations of the few times cycled configurations.

Table 1: Combined APE-smearing parameters to fit the cycled configurations.

mapping to:	$\{W_1\}$	$\{W_2\}$	$\{W_3\}$	$\{W_4\}$	$\{W_5\}$	$\{W_6\}$
$\sum c_i$	1.1	2.2	3.6	4.5	5.5	6.5
σ^2	0.01	0.01	0.01	0.008	0.008	0.008
mapping to:	$\{W_7\}$	$\{W_8\}$	$\{W_9\}$	$\{W_{10}\}$	$\{W_{11}\}$	$\{W_{12}\}$
$\sum c_i$	7.4	8.4	9.3	10.4	11.4	12.4
σ^2	0.008	0.007	0.007	0.007	0.007	0.007

2.3   Comparing Cycling and RG mapping

The ultimate test of the RG mapping is the comparison of the topological properties of the cycled and RG mapped lattices. We used the 20 8^4 lattices described above for this test. We cycled the configurations up to 12 times and measured the topological density using the algebraic operator defined in [9]. We also measured the total charge using the geometric operator. Next we RG mapped the original configurations using consecutive APE steps each with parameter $c \leq 0.45$ as described in Table 1. We analyzed the RG mapped configurations the same way as the cycled ones.

The instantons on these configurations have radii around $\rho = 2a$, sometimes even less. When instantons are as small as these ones, their radius is quite

uncertain. A radius 1.5 instanton centered at a lattice site shows up quite differently from one centered in the middle of a hypercube. We will analyze small smooth instantons in Section 3.1. Based on those results we note that instanton sizes around $\rho = 2a$ are trustworthy only up to 10-20%.

Here we consider in detail two sample configurations, a "nice" one and a "complicated" one. Configurations cycled less than 5-6 times are usually too rough to get a reliable estimate of the instanton content. Table 2 lists the instanton content of the "nice" configuration after 6, 9 and 12 cycling and RG mapping steps. The table also lists the topological charge measured by the algebraic operator (the geometric operator gave results which were consistent with the algebraic operator) and the locations and radii of the instantons (I) and anti-instantons (A) as well. The instanton content of the cycled and fitted configurations are identical for cycling steps 9 and 12 - the locations agree exactly and the radii agree within 10%. (Considering the difficulty in identifying small instantons, 10% agreement in the radii is actually better than expected.) On the 6 times RG mapped configuration we found an extra instanton-anti-instanton pair. These two objects are very close, about 2.5 lattice units or 50% of their combined radii. It is not obvious if they are the artifact of the instanton finder on a rough configuration or if they are indeed present on the configuration but both cycling and RG mapping annihilate them after a few steps. Since even in principle it is not possible to separate nearby pairs, we are not worried about the disappearance of this pair. In Section 3.1 we will study the properties of pairs in more detail.

Table 2: Instanton content of a "nice" 8^4 configuration

cycling	Cycled			Fitted		
	Q	ρ	location	Q	ρ	location
6	0.002	I 2.1	0,7,2,1	0.002	I 1.9	0,7,2,1
		A 2.2	7,1,1,6		A 2.0	7,1,1,6
					I 2.9	6,2,4,4
					A 2.3	5,2,6,5
9	0.001	I 2.3	0,7,2,1	0.001	I 2.1	0,7,2,1
		A 2.6	7,1,1,6		A 2.3	7,1,1,6
12	0.001	I 2.5	0,7,2,1	0.001	I 2.3	0,7,2,1
		A 2.8	7,1,1,6		A 2.6	7,1,1,6

Table 3 lists the the instantons found on the "complicated" configuration. That configuration has $Q = 1$ on the cycled lattices. After 6 cycling steps the instanton finder identifies 4 instantons and 3 anti-instantons. Three of the instantons have radii less than 2. We can identify these instantons by their location on the once cycled lattice where their radii are even smaller, 1.4, 1.5, 1.7, respectively. These instantons grow slowly under the cycling transforma-

tion. After 12 cycling steps we could identify only three of the four instantons and only one of the three anti-instantons. The missing instanton and one of the anti-instantons at locations (4,7,0,0) and (3,7,2,7) formed a close pair with distance about 2.5 lattice units or 65% of their combined radii on the 6 times cycled configuration. It is quite possible that they have annihilated. The second missing anti-instanton is probably still present as the topological charge on the lattice remained $Q = 1$. It most likely grew to a size comparable to the lattice itself ($\rho \approx 4$) and our instanton finder could not locate it. On the RG mapped configurations the topological charge was $Q = -2$. Comparing the instanton content of the 6 times cycled/RG mapped configurations, we see that the three small instantons did not survive the RG mapping transformation. The 4 objects that survived 6 RG mapping steps appear to be stable, they are present after 12 steps also. Small instantons are obviously sensitive to local transformations and can get lost, as this example shows.

Table 3: Instanton content of a "complicated" 8^4 configuration

cycling	Cycled			Fitted		
	Q	ρ	location	Q	ρ	location
6	1.09	I 1.6	4,6,3,0	-2.10		
		I 1.7	1,3,0,5			
		I 1.8	4,7,0,0			
		I 2.8	7,7,7,1		I 2.7	7,7,7,1
		A 2.1	3,7,2,7		A 2.1	3,7,1,7
		A 2.4	3,5,4,3		A 2.4	3,5,4,3
		A 2.9	0,4,5,7		A 3.1	1,5,4,6
12	1.04	I 1.9	4,6,3,0	-2.10		
		I 2.0	1,3,0,5			
		I 2.9	7,7,0,2		I 3.0	7,7,0,2
		A 2.6	4,5,3,3		A 2.5	4,5,3,3
					A 2.3	2,7,1,7
					A 3.7	2,4,6,6

A similar analysis can be performed on all the other configurations. The qualitative features are the same as on the sample configurations. If the instanton radius is larger than about 1.5 lattice units on the original lattice, the instanton is stable. It will survive the cycling as well as the RG mapping steps. The location of the instanton is usually unchanged (occasionally it is shifted by a lattice unit in one or more directions) and is identical on the RG mapped and cycled lattices. The radii of RG mapped and cycled lattices agree up to about 10%, better for larger instantons. The total topological charge is usually stable and identical on the cycled and RG mapped lattices. When there is a difference, we can identify the small instanton which was lost by one of the methods. The disappearance of a small instanton sometimes creates a localized roughness on

the configuration. When that happens the algebraic topological charge operator might give a value that is in between the old and new topological charge for a few cycling/RG mapping steps before settling down at the new topological charge value. Apart from these "transitional" cases the algebraic charge is close to an integer and it is also consistent with the geometric charge.

We have never observed the creation of an instanton between steps 6 and 12 as suggested by Ref. [8].

One feature that we observe both on the cycled and RG mapped lattices is that the instanton size changes slowly with increasing number of smoothing steps. It usually increases. If we want to measure the size distribution on the original lattice, we have to take this gradual change into account.

3   Properties of RG mapping

As we have demonstrated in Section 1, a series of APE-smearing steps approximates the cycling procedure closely. In this section we will study the behavior of smooth instantons, pairs, and Monte Carlo generated instantons under RG mapping. We will also investigate how RG mapping changes the short distance structure of the lattice.

As we pointed out in Section 1.2, the precise sequence of APE steps is not important. In the following we perform 12-60 APE-smearing steps with parameter $c = 0.45$ to emulate cycling steps 5-25. It is not important whether a certain number of APE smearing steps, like 24, corresponds to 11 or 12 cycling steps or somewhere in between, as we are monitoring the development of the configuration and will attempt to extrapolate it back to the original lattice or zero APE-smearing.

3.1   Properties of Smooth Instantons and Pairs under RG Mapping

We generated lattice configurations containing single instantons of various sizes by discretizing the continuum instanton solutions as described in Ref. [19]. Besides the instanton radius there is an additional parameter that might be important, especially for small instantons. This is the location of the instanton center with respect to the lattice. We chose to study the two extremes, i.e. instantons centered on a lattice site and centered in the center of a lattice cube.

We performed up to 60 $c = 0.45$ APE smearing steps on the single instanton configurations. All instantons with $\rho/a > 1.5$ survived 24 APE steps. We found that if the instantons were centered on a lattice site, then they could be safely identified even after 60 APE steps, provided their initial radius was $\rho/a > 1.25$. On the other hand for instantons centered in the middle of a hypercube, this happened only for $\rho/a > 2.25$. This shows that the fate of small instantons can be very sensitive to their location with respect to the lattice.

As an illustration, in Fig. 1 we show the APE evolution of the size of single instantons of radius 2 and 4 lattice spacings with the two different types of locations for their centers. In order to avoid finite size effects the radius 2 and 4 instantons were created on 8^4 and 16^4 lattices respectively. In all cases the instanton radius is shown in units of the corresponding initial continuum instanton radius (i.e. 2 and 4). We can see that larger instantons tend to change less during the process. For the $\rho/a = 2$ instanton there is a 20% difference in the observed initial radius depending on the location of the center, while for the $\rho/a = 4$ instanton that uncertainty is reduced to below 5%. A linear extrapolation of the size from 12-24 APE steps reproduces the size on the original lattice within a few percent for all instantons.

The reason that we predict the size of instantons centered at lattice sites better that those centered at the center of the hypercube is purely technical: our instanton finding algorithm compares every object to a smooth instanton centered at a lattice site.

We also observe that that these hand crafted instantons always shrink under APE smearing. This is expected since APE smearing is locally similar to cooling with the Wilson action, which is expected to shrink the instantons because smaller instantons have lower Wilson action. This is to be contrasted with the observation that on real Monte Carlo generated configurations only some of the instantons shrink, while most of them grow under APE smearing (see Section 3.2).

We also did some tests on how oppositely charged pairs behave under APE smearing. The pair configurations were produced by adding the logarithm of the links of appropriately shifted single instanton configurations and then re-exponentiating them. As long as the separation of the pair was bigger than the sum of the radii their sizes changed in essentially the same way as that of single instantons. Finally we also looked at a few configurations with more instantons, their locations and sizes taken from real many times cycled configurations. The picture we found was the same again as with single instantons; all the objects slowly shrank with a velocity depending on their size.
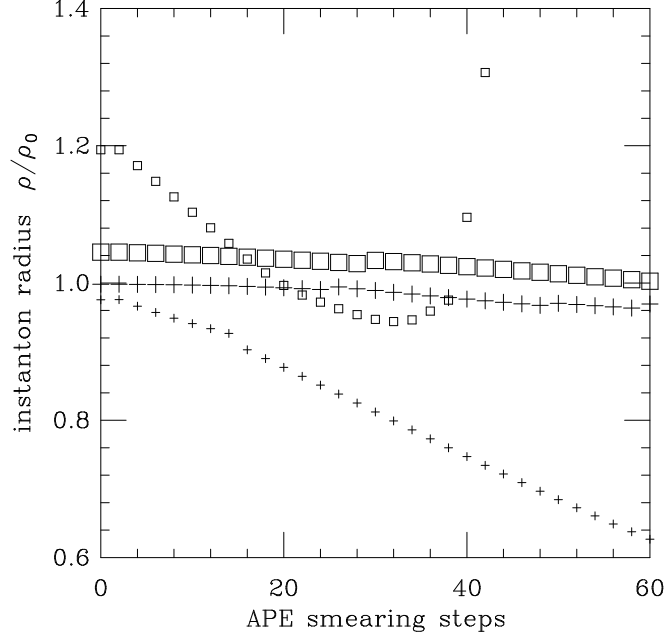
Figure 1: The "APE history" of a single instanton of radius $\rho = 2.0$ (small symbols) and $\rho = 4.0$ (large symbols) initially centered on a lattice site (pluses) and in the middle of a hypercube (squares). The small instantons are on 8^4 the big ones are on 16^4 lattices. The instanton radius is shown in units of the corresponding initial continuum instanton radius i.e. 2 and 4 lattice spacings.

3.2   Evolution of Monte Carlo Generated Instantons under RG Mapping

Smooth instantons of size $\rho/a > 1.5$ appear to be stable under RG mapping if no more than 20-30 APE-smearing steps are done with $c = 0.45$. The size of the instantons decreases with RG mapping but a linear extrapolation to the original lattice reproduces their size to 10-20% accuracy for larger/smaller instantons.

The preliminary analysis of Section 2.3 shows that Monte Carlo generated instantons of size $\rho/a > 1.5$ are also stable under RG mapping but these instantons usually grow under repeated APE-smearing.

In this section we consider a 16^4 configuration generated with Wilson action $\beta = 2.5$ (lattice spacing $a \approx 0.085$ fm) and study the evolution of instantons between 12 and 24 $c = 0.45$ APE-smearing steps. This configuration has a total charge $Q = 2$ on all the studied configurations. After 12 smearing steps, the instanton finder identified 7 instantons and 6 anti-instantons. On the 18 times smeared configuration only 4 instantons and 4 anti-instantons remain, and the same objects are observed even after 24 steps. Fig. 2 shows the size of the 8 "stable" objects as a function of the APE-smearing steps. From the 4 instantons (diamonds) 3 increase in size while one decreases, but all vary linearly with smearing steps. The slope of the linear change for all of them is smaller than 0.035. Three of the anti-instantons (bursts) behave similarly, though one has a slightly larger slope, 0.05. The fourth anti-instanton (crosses) starts to grow rapidly after 18 smearing steps and will disappear after a few more steps. This object is likely to be a vacuum fluctuation, not an instanton. Since the total charge is $Q = 2$ on these configurations, either the instanton identifier missed an instanton or one of the anti-instantons, probably the one with the largest slope, is also only a vacuum fluctuation.

We can conclude that the location of true topological objects is stable over many smearing steps and their size changes slowly though it can increase or decrease as well. To identify them on the lattice one has to track them over several smearing steps and monitor their behavior.

3.3   The Potential on RG Mapped Configurations

In our previous work we saw that cycling did not change the long distance features of the configurations and the string tension extracted from the heavy quark potential was essentially unchanged through 9 steps of cycling [9]. Here we performed the same test for the RG-mapping. In Fig. 3 we show the heavy quark potential extracted from timelike Wilson loops on the original configurations after 12 and 24 $c = 0.45$ APE smearing steps. The measurement was done on a set of 120 16^4 configurations generated at Wilson $\beta = 2.5$. The qualitative features are the same as for cycling. As expected, the short distance part of the potential is changed by APE smearing, and the potential is shifted down, but the string tension (the slope) is essentially unchanged.
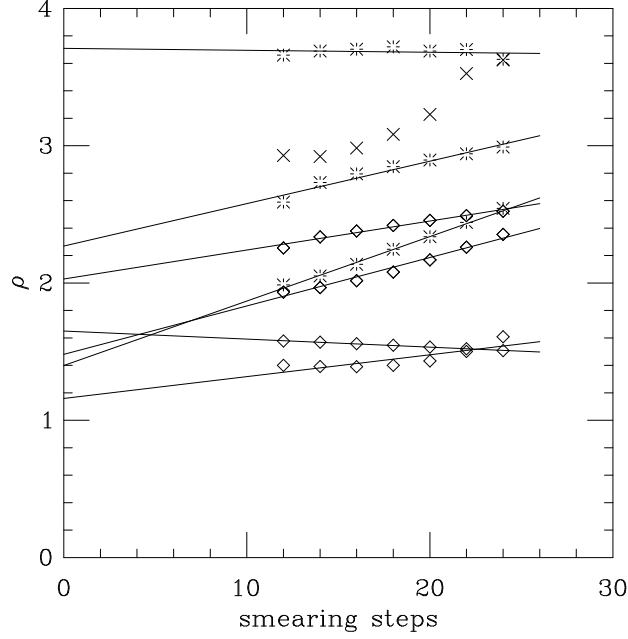
Figure 2: Radius versus APE-smearing steps of instantons (diamonds) and anti-instantons (bursts and crosses) on a 16^4 $\beta = 2.5$ configuration.

4 Results

One of our goals in this paper is to compare results obtained with the cycling/RG mapping method with results published using other algorithms [11, 12, 14]. Since most available data for topology was obtained using the Wilson gauge action, we will also use the Wilson action in the following. It is known that the Wilson action has poorer scaling in general and quite bad instanton scale invariance in particular. This is not a big problem if we compare results directly to others' calculations at identical coupling values. As far as scaling is concerned, we have to go to a large enough coupling where the scaling violations
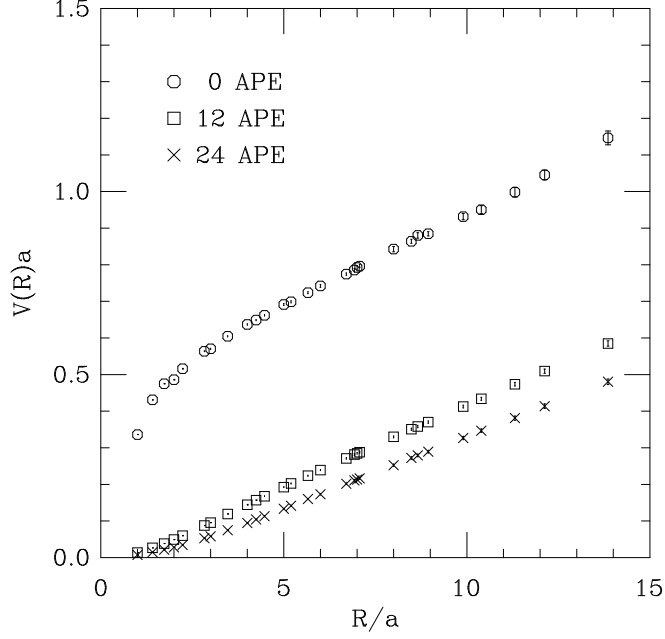
Figure 3: The heavy quark potential on a set of 120 16^4 configurations at Wilson $\beta = 2.5$ measured after 0 (octagons), 12 (squares) and 24 (crosses) $c = 0.45$ APE smearing steps.

are negligible.

4.1 Parameters of the Simulation

We have performed simulation at $\beta = 2.4, 2.5$ and 2.6. The parameters of the simulations are given in Table 4. The configurations were separated by 100 (at $\beta = 2.4$), 150 (at $\beta = 2.5$) and 200 (at $\beta = 2.6$) sweeps and all our lattices are periodic. The lattice spacing in Table 4 was calculated using the string tension

results of [20, 21] and the phenomenological formula of [22]. Our statistics are about double that of Ref. [12].

Table 4: Parameters of the simulations

β	L	number of configurations	a [fm]	La [fm]
2.4	12	397	0.1210(1)	1.45
2.4	20	28	0.1210(1)	2.42
2.5	16	218	0.0850(5)	1.36
2.6	20	370	0.061(2)	1.22

4.2 The Topological Susceptibility

We have measured the topological charge using the FP algebraic operator [9] after 12, 18 and 24 $c = 0.45$ APE-smearing steps. In addition, on the $\beta = 2.5$ configurations we also measured the charge using the geometric topological operator after 12 smearing steps. Table 5 contains our results for $\langle Q^2 \rangle$ and $\chi^{1/4}$. The quoted errors in $\chi^{1/4}$ are due to the statistical error of $\langle Q^2 \rangle$. The error due to the uncertainty of the lattice spacing is negligible for $\beta = 2.4$ and 2.5, but at $\beta = 2.6$ it is about 3 per cent, significantly contributing to the error of $\chi^{1/4}$. The second error at $\beta = 2.6$ indicates the uncertainty due to the lattice spacing. At $\beta = 2.4$ we quote $\langle Q^2 \rangle$ only from the 12^4 configurations. We have only 28 configurations on the 20^4 lattices. While the total volume of these configurations is comparable to the small lattice runs, it is not sufficient to get a statistically meaningful value for the susceptibility.

We observe, as expected, a small systematic decrease in the susceptibility as we increase the number of smearing steps. At large β the change is small and statistically insignificant. Only at $\beta = 2.4$, where the configurations are the roughest, do the 12 and 24 smearing steps results differ by about a standard deviation.

Fig. 4 shows the variation in $\langle Q^2 \rangle$ with smoothing steps at $\beta = 2.4$ and 2.6. The change occurs because instantons are lost under smoothing. Since the susceptibilities measured on the same set of configurations after different numbers of smearing steps are correlated, in spite of the statistical errors it is still meaningful to extrapolate them to 0 smearing step. These extrapolated values are also quoted in Table 5. With the extrapolation we take into account the contribution of instantons that are lost during the smoothing steps, either because they were too small, and smoothing washed them away, or because they were too large, and during repeated smoothing they grew out of the lattice. The

16

Table 5: Results for the susceptibility

β	L	smearing	$\langle Q^2 \rangle$	$\chi^{1/4}$[MeV]
2.4	12	12	5.2(4)	206(5)
		18	4.8(4)	204(5)
		24	4.5(3)	200(5)
		extrapolated to 0	5.9(4)	211(5)
	8	other	0.86(13)	197(7)
2.5	16	12(geom)	5.4(5)	221(5)
		12(alg)	5.4(5)	221(5)
		18	5.2(5)	218(6)
		24	5.1(5)	217(6)
		extrapolated to 0	5.5(5)	222(6)
2.5115	12	other	1.5(2)	221(7)
2.6	20	12	3.3(3)	218(8)(7)
		18	3.3(3)	218(10)(7)
		24	3.2(2)	216(10)(7)
		extrapolated to 0	3.4(3)	220(10)(7)
	16	other	1.26(15)	214(7)(7)

extrapolation cannot account for instantons that are too small to be present even on the original, unsmoothed lattice. The susceptibility increases by 10% from $\beta = 2.4$ to $\beta = 2.5$ but stabilizes after that at the value $\chi^{1/4} = 220(6)$ MeV. We interpret the change between the extrapolated $\beta = 2.4$ result and the larger β results as due to the absence of small instantons at $\beta = 2.4$ because of the larger lattice spacing. This interpretation will be supported by the instanton size distribution result discussed in Section 4.3. The result for the susceptibility is consistent with our earlier results [6],[9] where we found $\chi^{1/4} = 230(10)$ MeV using the cycling method with the FP action on much rougher lattices.

Table 5 contains another set of results for $\langle Q^2 \rangle$ and $\chi^{1/4}$ marked "other". Those were obtained using an earlier, unpublished version of the RG mapping algorithm. That mapping used about 50 paths to map the original configuration to the cycled one obtained with the shifted blocking procedure. We have not tested that algorithm in such detail as the present one, but preliminary results indicate that it has about the same minimum instanton size as the present algorithm. The agreement between the results supports this expectation and also indicates that finite size effects are indeed small.

We can compare the data for $\langle Q^2 \rangle$ with the result published in Ref. [12]. They quote the susceptibility after 20, 50, 150 and 300 improved cooling steps. The general trend is that the susceptibility slowly decreases during cooling but the change slows down with more cooling. For example at $\beta = 2.4$ the "cool-
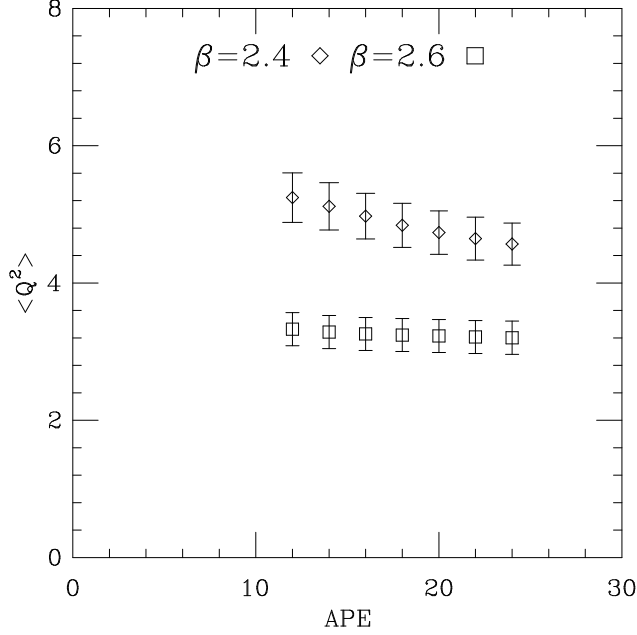
Figure 4: The susceptibility $\langle Q^2 \rangle$ vs number of $c = 0.45$ APE steps. Symbols are diamonds for $\beta = 2.4$ and squares for $\beta = 2.6$.

ing history" of $\langle Q^2 \rangle$ is 4.5(3), 4.4(3), 4.2(3), 4.0(3) for 20, 50, 150 and 300 cooling steps. The change in the susceptibility is comparable or smaller than its statistical error and the authors of [12] consider that $\langle Q^2 \rangle$ stabilizes after $O(100)$ cooling steps. At $\beta = 2.4$ on the same lattice size as Ref. [12] we found $\langle Q^2 \rangle = 4.5(3)$ after 24 APE steps. This result is somewhat larger than, but consistent with [12]. However our zero smearing step extrapolated number, $\langle Q^2 \rangle = 5.9(4)$ is several standard deviations different from the result of [12] even if we consider their $\langle Q^2 \rangle$ after 20 cooling sweeps. At $\beta = 2.5$ only a small data set on 12^4 lattices was used in [12]. The published result for the susceptibility is $\chi^{1/4} = 217(7)$ MeV indicating $\langle Q^2 \rangle = 1.45(20)$. Rescaling with the volume so it corresponds to our lattice size predicts $\langle Q^2 \rangle|_{16^4} = 4.6(6)$, again

lower than, but consistent with, our 24 APE steps result but two standard deviation different than our extrapolated result. At $\beta = 2.6$ in Ref. [12] 24^4 lattices with twisted boundary condition were used. The published result for the charge is $\langle Q^2 \rangle = 4.2(7)$ (after 150 cooling steps). Rescaling with the volume factor translates to $\langle Q^2 \rangle|_{20^4} = 2.0(3)$ on a 20^4 lattice. This number is 50% lower and 3 standard deviations away from ours. Finite size effects cannot explain the difference as they would push our numbers even higher. We do not understand the reason of this discrepancy, especially not why it shows up only at the largest coupling value.

In the remainder of this section we will discuss the relation between the algebraic and geometric definition of the topological charge and the possibility of a non-trivial renormalization group factor in the definition of the topological susceptibility [13].

First, we compare the geometric and algebraic charges on the 12 times smeared $\beta = 2.5$ lattices. $\langle Q^2 \rangle$ agrees with the two methods, but we can compare the charges measured on the individual configurations as well. Since the algebraic charge does not give an integer value, we compare the geometric charge to the nearest integer of the algebraic charge for the first 50 of the $\beta = 2.5$ configurations (Figure 5). Here the diamonds correspond to the geometric charge and the bursts to the integer algebraic charge. The two agrees most of the time, occasionally differing by one. The crosses in Figure 5 correspond to the original, non-integer value. They are usually close to an integer, and when the geometric and the integer algebraic charges are different, the original value is in between the two.

Just how close is the algebraic charge to an integer? To quantify that, we use the following three quantities

$$
\begin{aligned}
\langle (\Delta Q)^2 \rangle &= \langle (Q^{int} - Q)^2 \rangle, \\
Z^2 &= \langle Q/Q^{int} \rangle \quad \text{if} \quad Q^{int} \neq 0, \\
M &= \langle Q^2 \rangle \quad \text{if} \quad Q^{int} = 0,
\end{aligned}
\tag{3}
$$

where Q^{int} is the nearest integer to the algebraic charge Q. The last two quantities correspond to the renormalization factors of Ref. [13, 14] if we assume Q^{int} is the true topological charge. It is expected that a scale invariant charge operator which gives close to integer values on smooth instantons, as ours does, has $Z = 1, M = 0$ on highly smoothed configurations. At $\beta = 2.5$ after 24 smearing steps we find

$$
\langle (\Delta Q)^2 \rangle = 0.03(1), \quad Z^2 = 1.01(1), \quad M = 0.02(1),
\tag{4}
$$

and at $\beta = 2.6$

$$
\langle (\Delta Q)^2 \rangle = 0.02(1), \quad Z^2 = 1.02(1), \quad M = 0.01(1),
\tag{5}
$$

19

consistent with this expectation. Since the measured susceptibility is consistent after 12,18 and 24 smearing steps, we expect similar results for Z^2 and M after 12 steps as well. Indeed, after 12 smearing steps the corresponding values at $\beta = 2.5$ are

$$\langle(\Delta Q)^2\rangle = 0.07(2), \quad Z^2 = 0.98(1), \quad M = 0.07(2), \tag{6}$$

and at $\beta = 2.6$

$$\langle(\Delta Q)^2\rangle = 0.04(2), \quad Z^2 = 1.01(1), \quad M = 0.04(1), \tag{7}$$

indicating that if there is any renormalization necessary of the topological susceptibility, it is very small. The above argument is based on the assumption that Q^{int} is the true charge of the configuration. We cannot disprove the possibility that even though the algebraic topological charge is close to an integer value $(\langle(\Delta Q)^2\rangle = 0.03 - 0.07)$, the true topological charge differs from it by some overall multiplicative renormalization factor, but we find this possibility unlikely.

4.3   The Instanton Size Distribution

We have identified individual instantons after every 2 APE-smearing steps between 12 and 24 steps. Since these configurations are still rough, many of the objects identified as instantons are in fact vacuum fluctuations and disappear after more smoothing steps. This is best illustrated if we calculate the topological susceptibility obtained using $I - A$, the difference between the number of instantons and anti-instantons on a given configurations as the charge operator. For example at $\beta = 2.5$ we find $\langle(I - A)^2\rangle = 11.1$ after 12, 8.8 after 18, and 8.3 after 24 smearing steps - 1.5 to 2 times larger than the direct measurement of $\langle Q^2\rangle$ on the same lattices.

An option is to smooth the lattice further. However we would like to keep the smoothing steps small to minimize the distortion of the lattice, like losing instantons and changing the size of instantons. Figure 6 shows the observed instanton size distribution on the 12 and 24 times smeared lattices at $\beta = 2.5$. For comparison we also plot the result of Ref. [11] which corresponds, in our normalization, to about 100 times smeared lattices. It is obvious from the figure that the total number of identified objects decreases as we increase the smoothing. The density of identified objects is 4.6 per fm^4 after 12 smearing steps, 3.0 fm^4 after 24 smearing steps, and about 2 per fm^4 in Ref. [11]. These density values are considerably larger than the expected value of about 1 per fm^4. The maximum of all 3 distributions is around $\bar{\rho} \approx 0.3$ fm, but that does not mean that on the original lattice $\bar{\rho} \approx 0.3$ fm since instantons usually grow
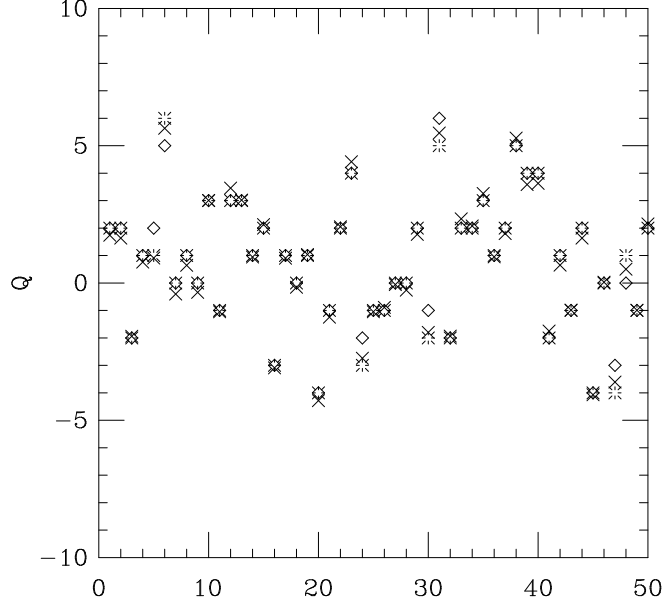
20

Figure 5: The geometric (diamonds) and algebraic (crosses) charge on a sequence of $\beta = 2.5$ 12 times smeared configurations. Since the algebraic charge is not integer, for clarity we plot the nearest integer value (bursts) also.

under smearing. This growth can also be observed from the increasing tail of the distribution, especially after the many blocking steps of [11].

What are these objects that disappear after repeated smearing steps but contaminate the result if we smear only 20-30 times? A few of them are genuine instantons, but most of them are vacuum fluctuations that the instanton finder erroneously identifies as topological objects. Some of these vacuum fluctuations could be nearby instanton - anti-instanton pairs. The topological susceptibility from $\langle (I - A)^2 \rangle$ is quite different form the reliable, direct measurements, indicating that most of the extra objects are only vacuum fluctuations. Our method
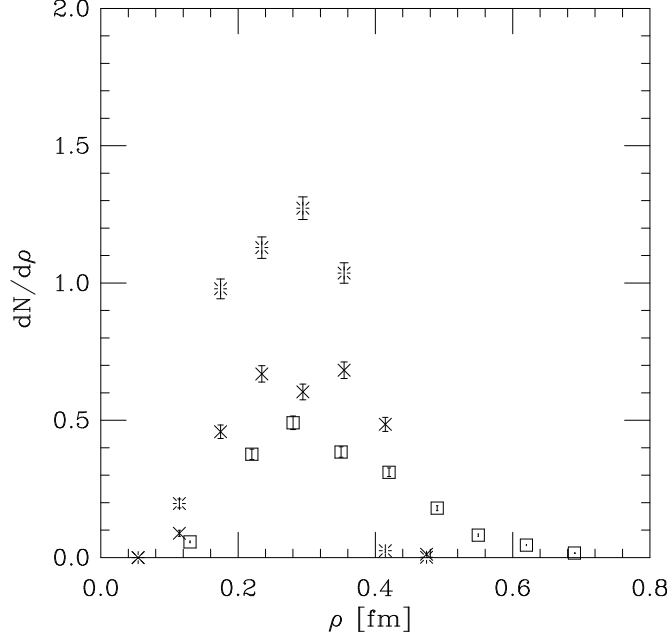
21

Figure 6: The size distribution on 12 (bursts) and 24 (crosses) times APE smeared lattices at $\beta = 2.5$. The square symbols are the results of Ref. [11] rescaled appropriately.

to distinguish true topological objects from vacuum fluctuations is to track individual objects during smearing. If an object is present over many smearing steps with slowly changing radius, we identify it as a topological object.

At smaller coupling values $\beta = 2.4 - 2.5$ we found that 12 to 18 $c = 0.45$ smearing steps were sufficient, but at $\beta = 2.6$ we needed 16 to 24 steps to smooth the configuration so larger instantons emerged from the vacuum fluctuations. The necessary smearing steps would increase further if we were to consider even larger couplings but as large instantons are affected less by the smoothing, that would not influence the result.

In the following analysis we identified instantons on configurations that had been APE smeared 16, 18, 20, 22 and 24 times with $c = 0.45$, and extrapolated their size linearly to zero smearing level. We kept only instantons where the slope of the linear extrapolation was less that 0.035. This cut was chosen such that the final distribution at each β value reproduced the topological suscepti-bility correctly, $\langle (I - A)^2 \rangle = \langle Q^2 \rangle$. With this cut the instanton density is 1.2 per fm^4 at $\beta = 2.4$ and 1.5 per fm^4 at $\beta = 2.5$ and 2.6. Again, we see that at the smallest coupling value some instantons are missing. These densities are 15-20% lower than the one we quoted in [9]. A reason for the discrepancy is that in [9] we used a 50% larger cut in the slope of the linear extrapolation. (Our statistics was not sufficient to adjust the cut to give the correct topological susceptibility.) We want to emphasize that our result for the instanton density, 1.5 per fm^4 is not a direct measurement. It is the result of combining 5 different APE smeared lattices and identifying those objects that are present and stable on all of them.

It is interesting to compare these densities with the results of Ref. [12]. Table 3.3.2 of [12] contains raw data for the instanton distribution from which one can calculate the instanton density. At $\beta = 2.4$ after 20 cooling sweeps the density is 2.5 per fm^4, and after 300 sweeps it is 0.5 per fm^4. A density of 2.5 per fm^4 is quite a bit larger than the phenomenologically expected value and probably contains a lot of vacuum fluctuations or instanton-anti-instanton pairs which are too close to distinguish them from vacuum fluctuations. On the other hand the density 0.5 per fm^4 is 2-3 times smaller than expected, indicating that cooling destroyed not only vacuum fluctuations but a lot of topological objects as well. It is not obvious to us why these two very different sets of configurations have the same instanton size distribution as it was found in Ref. [12]. The densities at $\beta = 2.6$ show a similar trend. After 50 sweeps the density is large, 3.7 per fm^4, and it drops to 0.9 per fm^4 after 300 sweeps.

Our final result for the instanton size distribution is shown in Figure 7, where we overlay the data obtained at $\beta = 2.4$ (octagons on 12^4, squares on 20^4 lattices), $\beta = 2.5$ (diamonds), and $\beta = 2.6$ (bursts). The bin size is 0.06 fm and the distribution $d\rho/dN$ is measured in fm^{-4}. Since the smoothing method cannot identify instantons with $\rho < 1.5a$, we chose the bins such that the second bin for each distribution starts at $\rho = 1.6a$. That means that we expect the second bin of each distribution to be universal, which appears to be true where we can check it, i.e. for the $\beta = 2.4$ and 2.5 distributions. The first bins on the other hand contain only some of the small instantons and their value is not expected to be universal.

The four distributions form a universal curve indicating scaling. The $\beta = 2.4$ curves cover only the $\rho > 0.2$ fm region, and small instantons are obviously miss-ing. The agreement between the 12^4 and 20^4 configurations at $\beta = 2.4$ indicate that a linear size of about 1.4 fm is sufficient to observe all the topological ob-
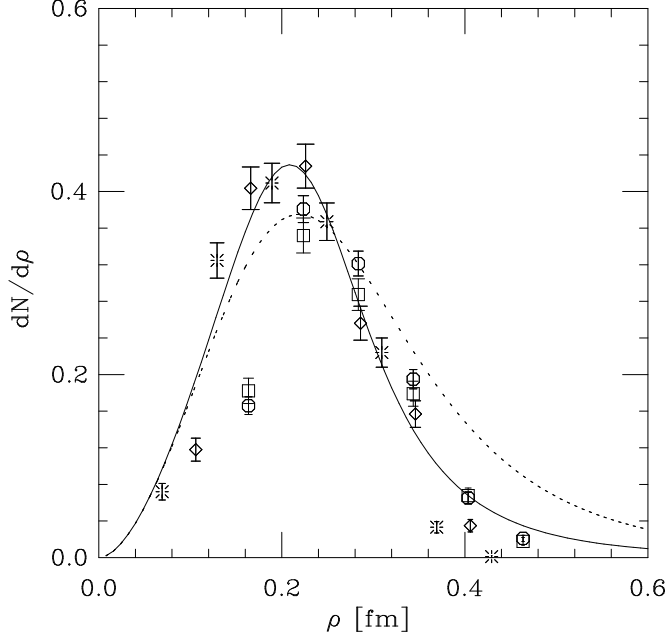
Figure 7: The size distribution of instantons. Octagons correspond to $\beta = 2.4$ 12^4, squares to $\beta = 2.4$ 20^4, diamonds to $\beta = 2.5$ and bursts to $\beta = 2.6$. The first bin of each distribution is contaminated by the cut-off. The solid curve is a two parameter fit to the data points according to the formula in Ref. [23] The dashed curve is a similar fit from Ref. [23] which describes the instanton liquid model quite closely.

jects. The $\beta = 2.5$ and 2.6 distributions have most of the physically relevant instantons supporting the scaling behavior observed for the topological susceptibility. It is possible, though statistically not significant, that we see some finite size effects for $\rho > 0.36$ fm at the $\beta = 2.6$ distribution. It is plausible that objects which are larger in diameter than about 0.8 fm will grow and after 16-24 APE-smearing steps become too big to be observed on a lattice of size 1.22 fm.

Our instanton size distribution is very different from the result of Ref. [12]. Their distribution peaks at $\rho = 0.43$ fm and they found hardly any objects with $\rho < 0.2$ fm. However, the instanton liquid model predicts a very similar picture to ours. In the interacting instanton liquid model Shuryak predicted an instanton size distribution that peaked around $\rho = 0.2$ fm [23]. In that paper the instanton distribution of [11] was fitted using the two loop perturbative instanton distribution formula with a "regularized" log

$$S_I = \frac{8\pi^2}{g^2(\rho)} = b_0 L + b_1 \log L \tag{8}$$

$$L = \frac{1}{p} \log[(\rho \Lambda_{inst})^{-p} + C^p] \tag{9}$$

where b_0 and b_1 are the first two coefficients of the perturbative β function and p and C are arbitrary parameters. For SU(2) $\Lambda_{inst} = 0.66$ fm and the best fit for the data of Ref. [11] gives $p = 3.5$, $C = 4.8$. The best fit for our data requires different values, $p = 6.4$, $C = 5.95$. The solid curve in Figure 7 corresponds to the latter fit while the dashed curve is the fit given in Ref. [23] that describes the instanton liquid model quite closely. The difference between the two fits is significant at large ρ values only. Our distribution and the corresponding fit cuts off much faster at large instanton sizes than the instanton liquid model prediction. A natural explanation would be that finite size effects in our simulations cause the Monte Carlo distribution to drop too fast at large ρ. However we compared distributions at linear lattice sizes 1.44 fm and 2.42 fm and observed no difference, so this explanation does not appear to be true. We do not know if changing the parameters of the interacting instanton liquid model slightly would change the predictions of that model improving the agreement with the Monte Carlo data.

In Ref. [9] we published a similar size distribution curve obtained by the cycling method on much rougher lattices using the FP action. That distribution agrees with the present one for $\rho < 0.35$ fm but is slightly larger for $\rho > 0.35$ fm. The reason for this difference is probably the same that caused the slightly larger overall density.

5   Summary of the RG Mapping Method

Our RG mapping method is a series of APE-smearing transformations. With smearing parameter $c = 0.45$ we found that the topological charge can be reliably measured after 12 to 16 smearing steps (slightly more at smaller β values). Individual instantons can be identified also after about 12 steps but to reliably distinguish them from vacuum fluctuations it is necessary to monitor them over

several smearing steps. Since instanton sizes change during RG mapping, tracking them over several smearing steps is also necessary so we can extrapolate their size to the original lattice. The smearing steps destroy the short distance properties of the lattice. The 12 to 24 steps that we are doing destroys structure on the lattice up to a few lattice spacings. As the lattice spacing decreases, this lattice short distance distortion becomes negligible.

APE smearing as a smoothing method for topology is not new. The Pisa group [13] has been using it for several years now. They usually do 2 APE-smearing steps with $c \approx 0.9$. This corresponds to about 4 of our smearing steps or two RG mapping steps. These configurations are not smooth enough for us to measure the topological charge directly. The Pisa group corrects for the vacuum fluctuations by a multiplicative and an additive renormalization factor. These renormalization factors also, in principle, partially correct for the fact that the naive twisted plaquette $F\tilde{F}$ operator used in most of their studies, gives the topological charge of small instantons quite poorly [19].

The "calibrated cooling" method of Michael and Spencer [11] is very similar to APE-smearing, except that the lattice is updated continuously during the transformation. They chose a smearing parameter $c = 0.75$ and performed 60-80 steps. That corresponds to over 100 steps in our notation. That many steps destroys many more instantons and most importantly, the size of the instantons can grow considerably. $O(100)$ smearing steps can also influence the short distance properties of the lattice considerably.

Our method differs from the above two in the following:

- It was motivated by and tested against the RG cycling transformation.

- We do enough smearing steps to be able to use an algebraic charge operator that gives close to integer values.

- We monitor that the long distance properties of the lattice are unchanged. The smearing steps destroy correlations at only a few (1-2) lattice spacings.

- We monitor individual instantons over several smearing steps to distinguish them from vacuum fluctuations. We also monitor their size and extrapolate it back to the original lattice.

We used Wilson action at several coupling values in our numerical simulation. We found that the topological susceptibility showed scaling for $\beta \geq 2.5$, and $\chi^{1/4} = 220(6)$ MeV. The instanton density (instantons and anti-instantons combined) is 1.5 fm^{-4}, and the instanton size distribution peaks at $\bar{\rho} = 0.2$ fm as shown in figure 7. A similar technique for $SU(3)$ gauge theory is under

development. This method of removing short distance fluctuations is very fast and easy to implement, but its price is that all observables must be carefully monitored over the history of processing steps and, if necessary, extrapolated back to zero steps.

Acknowledgements

References

[1] D. Diakanov, Lectures at the Enrico Fermi School in Physics, Varenna, 1995, hep-ph/9602375.

[2] T. Schäfer and E. V. Shuryak, "Instantons in QCD," hep-ph/9610451.

[3] S. Weinberg, Phys. Rev. D11 (1975) 3583; G. t'Hooft, Phys. Rev. D14 (1976) 3432; Phys. Rev. Lett. 37 (1976) 8.

[4] E. Witten, Nucl. Phys. B156 (1979) 269; G. Veneziano, Nucl. Phys. B159 (1979) 213.

[5] M. Blatter, R. Burkhalter, P. Hasenfratz and F. Niedermayer, Nucl. Phys. **B** (Proc. Suppl.) 42 (1995) 799; M. Blatter, R. Burkhalter, P. Hasenfratz and F. Niedermayer, Phys. Rev. D53 (1996) 923. R. Burkhalter, Phys. Rev. D54 (1996) 4121.

[6] T. DeGrand, A. Hasenfratz, D. Zhu, Nucl. Phys. B478 (1996) 349.

[7] R. Narayanan and H. Neuberger, Nucl. Phys. B412 (1994) 574; R. Narayanan, and P. Vranas, preprint UW-PT-97-04 and hep-lat/9702005.

[8] R. Narayanan and R. Singleton, talk presented at Lattice '96, hep-lat/9709014.

[9] T. DeGrand, A. Hasenfratz,T. Kovács, The Topological Structure in the SU(2) Vacuum, preprint COLO-HEP-383 and hep-lat/9705009, in press, Nucl. Phys. B.

[10] D. J. R. Pugh, M. Teper, Phys. Lett. B218 (1989) 326; M. Teper, hep-lat/9711011 and OUTP-97-62P (Lectures given at NATO Advanced Study Institute on Confinement, Duality and Nonperturbative Aspects of QCD).

[11] C. Michael and P.S. Spencer, Phys. Rev. D52 (1995) 4691.

[12] Ph. de Forcrand, M. Garcia Perez and I.-O. Stamatescu, hep-lat/9701012.

[13] A. Di Giacomo, E. Vicari, Phys. Lett. B275 (1992) 429; B. Alles, M. Campostrini, A. Di Giacomo, Y. Gündüc, and E. Vicari, Phys. Rev. D48 (1993) 2284; C. Christou, A. Di Giacomo, H. Panagopoulos and E. Vicari, Phys. Rev. D53 (1996) 2619.

[14] B. Alles, M. D'Elia, and A. Di Giacomo, hep-lat/9706016.

[15] P. Hasenfratz, and F. Niedermayer, Nucl. Phys. B414 (1994) 785.

[16] T. DeGrand,A. Hasenfratz, P. Hasenfratz, F. Niedermayer, Nucl. Phys. B454 (1995) 587.

[17] T. DeGrand,A. Hasenfratz, P. Hasenfratz, F. Niedermayer, Nucl. Phys. B454 (1995) 615.

[18] M. Falcioni, M. Paciello, G. Parisi, B. Taglienti, Nucl. Phys. B251[FS13] (1985) 624. M. Albanese, et al. Phys. Lett. B192 (1987) 163.

[19] T. DeGrand, A. Hasenfratz, D. Zhu, Nucl. Phys., B475 (1996) 321.

[20] J. Fingberg, U. Heller, and F. Karsch, Nucl. Phys. B392 (1993) 493.

[21] G.S. Bali, K. Schilling, C. Schlichter, Phys. Rev. D51 (1995) 5165.

[22] UKQCD Collaboration (S.P. Booth et al.), Phys. Lett. B275 (1992) 424.

[23] E. V. Shuryak, Phys. Rev. D52 (1995) 5730; Nucl. Phys. B302 (1988) 574.